Relativistic configuration interaction calculations for polyatomics: Applications to PbH2, SnH2, and GeH2

K. Balasubramanian

Citation: The Journal of Chemical Physics **89**, 5731 (1988); doi: 10.1063/1.455583
View online: http://dx.doi.org/10.1063/1.455583
View Table of Contents: http://scitation.aip.org/content/aip/journal/jcp/89/9?ver=pdfcov
Published by the AIP Publishing

Relativistic configuration interaction calculations for polyatomics: Applications to PbH_2, SnH_2, and GeH_2

K. Balasubramanian[a)]
Department of Chemistry, Arizona State University, Tempe, Arizona 85287-1604

(Received 25 April 1988; accepted 27 July 1988)

A relativistic configuration interaction scheme is described for polyatomic molecules containing heavy atoms. In this method first complete active space MCSCF followed by large scale configuration interaction calculations are carried out. The natural orbitals generated in the large scale CI are then used in the relativistic CI (RCI) calculations, which include the spin–orbit integrals. The spin–orbit integrals are obtained using large Gaussian basis sets, with the operator expressed as a difference of relativistic effective core potentials, and then transformed over the natural orbitals. The transformed integrals are included as one-electron matrix elements in the RCI. This procedure thus takes into account both electron correlation and spin–orbit effects. The method is applied to the spin–orbit states derived from the three low-lying states of PbH_2, SnH_2, and GeH_2 ($^1A_1$, $^3B_1$, and $^1B_1$). The spin–orbit mixings of the $^1A_1$ and $^3B_1(A_1)$ states in the RCI wave functions of PbH_2 and SnH_2 were found to be quite significant. For PbH_2 this mixing lowers the $^1A_1$ state by 1308 cm^{-1} while the $^3B_1(A_1)$ is raised by 1371 cm^{-1} with respect to the $^3B_1$ state without the spin–orbit splitting. The dipole moments of all the three radicals reveal that PbH_2 has the largest dipole moment of the three. The electronic states of GeH_2 and SnH_2 are similar [$^1A_1(A_1) - {}^3B_1(A_1)$:$T_e$ = 23.1 kcal/mol for GeH_2, T_e = 23.8 kcal/mol for SnH_2], but the electronic states of PbH_2 differ [$^1A_1(A_1)$–$^3B_1(A_1)$:T_e = 41 kcal/mol] from their lighter analogs in that the splittings of the excited states are considerably higher. The Mulliken population analyses of the CI natural orbitals reveal that this is primarily a result of the relativistic stabilization of the 6*s* orbital of the lead atom due to the mass–velocity contraction. The geometries of the A_1 component of the $^3B_1$ state are altered to a considerable extent by the spin–orbit term for both PbH_2 and SnH_2.

I. INTRODUCTION

The singlet–triplet splitting of methylene, CH_2, has been the subject of numerous investigations in the past two decades.[1,2] There have been similar investigations on the heavier species, namely SiH_2[3–5] and GeH_2.[6,7] The methylene radical has a triplet ground state X of $^3B_1$ symmetry and an excited $\mathbf{A}\ ^1A_1$ state. The $\mathbf{X}\ ^3B_1$–$\mathbf{A}\ ^1A_1$ splitting has been the subject of considerable controversy for many years. The latest experimental value[2] for this separation is 8.7 ± 0.5 kcal/mol while the best theoretical value is 9.8 kcal/mol.

The heavier analogs of methylene, namely SiH_2 and GeH_2, have also been studied to some extent[3–7]. For both SiH_2 and GeH_2, the $^1A_1$ and $^3B_1$ states are reversed in order with respect to CH_2. The $\mathbf{X}\ ^1A_1$–$\mathbf{a}\ ^3B_1$ splitting of SiH_2 is calculated to be about 21 ± 1 kcal/mol.[5] The corresponding splitting for GeH_2 without relativistic effects was calculated to be 22.5 kcal/mol.[6,7] The three electronic states of SnH_2 were studied by the present author[8] in the absence of spin–orbit effects. The singlet–triplet energy separation of SnH_2 in the absence of spin–orbit coupling was calculated to be 22.5 kcal/mol.[8] The general trend of the singlet–triplet splittings of CH_2–SnH_2 is discussed in Ref. 9. The remarkable similarity of the electronic states of GeH_2 and SnH_2 may tempt one to conclude that the $^1A_1$–$^3B_1$ splitting of PbH_2 should also be about 23 kcal/mol in the absence of spin–orbit effects. Even in the absence of spin–orbit effects the present investigation reveals that this separation is much larger for PbH_2 primarily due to the relativistic stabilization of the 6*s* orbital of the lead atom.

The electronic states of PbH_2 have not been investigated to date. This is primarily because of the large relativistic and spin–orbit effects. Further, the effects of spin–orbit coupling on the electronic states of PbH_2, SnH_2, and GeH_2 have not been investigated at all.

The dipole moment of the related GeH diatomic has been a subject of some controversy in recent years.[10–13] Theoretical calculations yield values in the neighborhood of 0.09 D while the reported experimental value is about 1.0 D.[10] Thus, the dipole moments of the electronic states of the bent GeH_2, SnH_2, and PbH_2 molecules would also be of considerable interest. We calculate the dipole moments of all three species in their low-lying electronic states.

The inclusion of spin–orbit effects for bent triatomics such as PbH_2, SnH_2, GeH_2, etc. require extension of our codes for relativistic CI (RCI) for diatomics which is carried out in a STO basis set. This code for diatomics is based on the general method described by Christiansen, Balasubramanian, and Pitzer.[14] Further extensions and enhancements of this procedure have enabled calculation of medium-scale RCI wave functions, dipole moments, and transition moments of electronic states of diatomic molecules containing very heavy atoms. These developments and results have been reviewed.[15]

The inclusion of the spin–orbit operator presents some

[a)] Alfred P. Sloan Fellow; Camille and Henry Dreyfus Teacher Scholar.

 0021-9606/88/215731-08$02.10

difficulties in the MCSCF or CI calculations. The spin–orbit operator mixes states of different spatial and spin symmetries. Thus conventional MCSCF or CI codes would not work if the spin–orbit matrix elements are introduced. For this reason the spin–orbit matrix elements are usually introduced as perturbations to the results of calculations without the spin–orbit term. This procedure would be adequate for lighter molecules. However, for molecules containing heavy atoms, since the mixing of different electronic states due to the spin–orbit term is large, a variational treatment such as relativistic CI is necessary. In this method, all configurations which mix in the presence of the spin–orbit term are included in the CI. In this investigation the spin–orbit matrix elements are obtained from *ab initio* relativistic effective potentials as differences of $l + 1/2$ and $l - 1/2$ potentials as suggested in Ref. 18 and included in the RCI calculations variationally. Hafner and Schwarz[19] have also suggested the use of differences of $l + 1/2$ and $l - 1/2$ semiempirical pseudopotentials as the spin–orbit operator.

One of the objectives of the present investigation is to describe a relativistic CI scheme for polyatomics which works in conjunction with large scale MCSCF/CI calculations. This scheme is then applied to calculate the properties of the electronic states of PbH_2, SnH_2, and GeH_2 including spin–orbit effects. The dipole moments of the various electronic states are also carried out. An extended (4*s*4*p*4*d* 1*f*) valence Gaussian basis set is employed for the heavy atom. Section II describes our method of investigation. Section III contains the results and discussions.

II. METHOD

The relativistic effective core potentials are obtained from the numerical Dirac–Hartree–Fock calculations by the methods described earlier.[16,17] The RECPs are averaged with respect to spin at the MCSCF and large scale CI calculational stages since this procedure enables treatment of the electronic states without the spin–orbit term.

The spin–orbit operator is derived from the RECPs as suggested by Ermler *et al.*[18] This operator is shown below:

$$H^{\mathrm{SO}} = \sum_{l=1}^{L} \Delta U_l^{\mathrm{REP}} \Bigg[\frac{l}{2l+1} \times \sum_{-l-1/2}^{l+1/2} |l,l+1/2,m\rangle\langle l,l+1/2,m| - \frac{l+1}{2l+1} \sum_{-l+1/2}^{l-1/2} |l,l-1/2,m\rangle\langle l,l-1/2,m| \Bigg],$$

$$\Delta U_l^{\mathrm{REP}} = U_{l,l+1/2}^{\mathrm{REP}} - U_{l,l-1/2}^{\mathrm{REP}}$$

where the $|l,l+1/2,m\rangle s$ are the two-component spinors.

Christiansen, Ermler, and co-workers[20–22] have recently generated Gaussian analytical fits for both the averaged RECPs and the spin–orbit operator suitable for molecular calculations. Pitzer and Winter[23] have developed codes to calculate the spin–orbit integrals from these Gaussian fits of the spin–orbit operator. We use Pitzer's modified version of the ARGOS codes to calculate the spin–orbit integrals over Gaussian basis sets.

The averaged RECPs are employed in MCSCF/CI calculations without the spin–orbit term. The MCSCF calculations carried out are complete active space MCSCF (CASSCF) calculations. In this method the valence electrons are distributed in all possible ways among a chosen set of the most important orbitals referred to as the active space. Large-scale configuration interaction calculations are carried out following the CASSCF procedure. The advantage of omitting the spin–orbit term at the large-scale CI levels of theories is that spin is still a good quantum number and consequently methods based on GUGA (graphical unitary group approach)[24–26] or the Liu–Yoshimine symbolic CI method[27] can be used. The MCSCF/CI methods described above are capable of accounting for correlation effects quite accurately.

The spin–orbit integrals are tranformed over the natural orbitals obtained from the MCSCF/CI methods without the spin–orbit term. The natural orbitals generated by the MCSCF/CI methods are superior to simple canonical virtual orbitals in that both the internal and external orbitals are improved by correlation effects. An ideal choice of orbitals would be the CASSCF orbitals for the internal space and CI natural orbitals for the external space. The diagonal elements of the transformed spin–orbit matrix in this space of orbitals would then provide a direct estimation of the first-order perturbative correction due to the spin–orbit operator for the open shell orbitals. The spin–orbit matrix constructed this way is superior to the ordinary spin–orbit matrix constructed from a single configuration SCF orbitals used up to now for diatomics since the orbitals used are much improved.

The transformed spin–orbit matrix elements are added to the one-electron matrix elements at the relativistic CI stage. The code developed earlier for diatomics was enhanced in many ways to carry out RCI for polyatomics. The integrals section of this code was interfaced with the transformation code for the polyatomic molecules. The symmetry group was changed to D_{2h} or its subgroups. At present the code is limited to about 25 000 configurations. We propose to extend this further by using the Liu–Davidson iterative diagonalization method which extracts the roots simultaneously.

A. Method of calculations for PbH_2, SnH_2, and GeH_2

Valence Gaussian basis sets of the type (4*s*4*p*4*d* 1*f*) are employed for the heavy atoms. These basis sets are shown in Table I. The 4*s*4*p*4*d* 1*f* basis sets are constructed by starting from the 3*s*3*p*3*d*, 3*s*3*p*4*d*, and 3*s*3*p*5*d* basis sets for Pb, Sn, and Ge, respectively, reported by Ermler and coworkers.[20–22] The 4*d* and 5*d* sets were contracted to 3*d* sets for Sn and Ge by contracting the large exponent *d* functions together. Diffuse sets of *s*, *p*, and *d* functions are added to this set. Then ten-component 4*f*-type Gaussian functions are added to the 4*s*4*p*4*d* set. The exponent for the 4*f*-type functions was optimized for the ground state of the molecule at its equilibrium geometry. These basis set sets were employed in both CASSCF and CI calculations but the CI calculations did not include *f* functions since the effect of *f* functions was found to be small.

TABLE I. Valence Gaussian basis sets employed[a] in this investigation for Ge, Sn, and Pb.

Type	Ge	Sn	Pb
s	1.018	0.554 1	0.6041
s	0.318 8	0.358 4	0.2863
s	0.103 0	0.093 8	0.0880
s	0.033 3	0.024 55	0.0270
p	1.836	0.927 0	0.7575
p	0.262 2	0.196 7	0.1843
p	0.079 76	0.064 2	0.0616
p	0.024 3	0.020 95	0.0206
d	44.88	3.120	1.5860
d	12.25	1.386 4	0.6013
d	3.832	0.605 3	0.2195
d	1.106	0.242 3	0.0801
d	0.320	0.097 0	...
d	0.093	...	...
f	0.40	0.46	0.45

[a] The first three *s*, *p*, and all but one *d* exponents were taken from Refs. 20–22. To this a diffuse *s*, and sets of *p*, *d* and *f*-type functions were added. The exponent of the *f* function was optimized for the ground state of the molecule.

We employ analytical Gaussian relativistic average potentials and the spin–orbit operators reported by Christiansen, Ermler, and co-workers[20–22] for Ge, Sn, and Pb. For all three elements the outermost $d^{10}s^2p^2$ shells were explicitly retained in the calculations, with the rest of the electrons replaced by relativistic effective core potentials.

The orbitals for CI calculations were generated using the complete active space MCSCF (CASSCF) method. The outer d^{10} shell was allowed to relax for all geometries in the CASSCF procedure, but electrons were not promoted from the *d* shell. The other six electrons were active in the CASSCF. The three a_1, two b_2, and one b_1 orbitals of MH_2 which correlated into the outer *s*, *p* orbitals of M and the 1*s* orbitals of the hydrogens were included in the CASSCF. The six active electrons of MH_2 were distributed in all possible ways among the orbitals in the active space.

The effects of *f*-type functions on the geometries of the ground states of MH_2 are summarized in Table II. As one can see, the *f* functions do not play a very significant role for these species. The bond contraction induced by *f* functions is largest for SnH_2 (0.003 Å). The bond angle increase is largest for PbH_2 (about 0.7°).

Configuration interaction (CI) calculations were made following the CASSCF. The configurations included in the CI calculations carried out for MH_2 were generated using the SOCI (second-order CI) method. The SOCI calculations included (i) all configurations in the CASSCF, (ii) configurations generated by distributing five electrons in the internal space and one electron in the orthogonal external space in all possible ways, and (iii) configurations generated by distributing four electrons in the internal space and two electrons in the external space in all possible ways. The dimensions of the CASSCF and SOCI calculations are shown in Table III. In addition, Davidson's corrections for higher-order unlinked cluster configurations not included in the SOCI were also calculated.[28]

The relativistic CI calculations were carried out following the CASSCF/CI calculations by the method described in Sec. II. The inclusion of the spin–orbit term in the Hamiltonian changes the single group symmetry into the spin double group. In general, all configurations which have the same symmetry in the spin double group mix in the RCI. The actual magnitude of mixing would depend on many factors including the separations of the various states in question. Table IV enumerates a list of possible low-lying configurations and the corresponding electronic states both in the C_{2v} and C_{2v}^2 groups for PbH_2, SnH_2, and GeH_2.

In the RCI calculations we included those configurations in the SOCI with coefficients $\geqslant 0.07$ for the appropriate state without the spin–orbit term as reference configurations. In addition, all possible states of different spatial and spin symmetries which are low-lying and which mix in the double group are included as reference configurations. Table V lists the actual reference configurations included for the various states. The convergence in the diagonalization of the RCI calculations was improved since the RCI calculations were carried out in the natural orbital basis sets generated from the SOCI calculations. This is the additional advantage of using the natural orbitals generated in the SOCI step.

Next, we discuss the spin functions for the various spatial configurations listed in Table V. The irreducible representations spanned by the three triplet functions in the C_{2v}^2 double group are obtained by correlating the three-dimensional rotation group irreducible representation $D^{(j)}$ ($j = 1$ for triplet) into the C_{2v}^2 double group. The result can be seen to be $A_2 + B_1 + B_2$. As Pitzer and Winter[23] showed, the $(\alpha\beta + \beta\alpha)/\sqrt{2}$ spin function transforms as A_2 while $(\alpha\alpha + \beta\beta)/\sqrt{2}$ and $(\alpha\alpha - \beta\beta)/\sqrt{2}$ transform as B_1 and B_2, respectively. Thus, for example, the leading configurations of the $^3B_1$ (A_2) in RCI would be $1a_1^2 2a_1\alpha 1b_2^2 1b_1\alpha$ and $1a_1^2 2a_1\beta 1b_2^2 1b_1\beta$. Note that the $^3B_1(A_2)$ and $^3B_1(A_1)$ would have the same leading reference configurations, the only difference being in their sign. The $^3B_1$ (B_2) state would

TABLE II. The effect of *f* functions for MH_2 ground state ($^1A_1$).

		CASSCF with *f* function		CASSCF without *f* function	
Molecule	State	r_e	θ_e	r_e	θ_e
GeH_2	$^1A_1$	1.604	92.9	1.605	92.8
SnH_2	$^1A_1$	1.800	92.4	1.803	92.1
PbH_2	$^1A_1$	1.917	91.6	1.919	90.9

TABLE III. The dimensions of the CASSCF and SOCI calculations.

State	CASSCF	SOCI
$^1A_1$	56	48 128
$^3B_1$	51	70 384
$^1B_1$	39	44 812

TABLE IV. List of various possible configurations and the corresponding electronic states in the C_{2v} and C_{2v}^2 groups.

Configuration	Electronic states	
	C_{2v}	C_{2v}^2
$1a_1^2 2a_1^2 1b_2^2$	$^1A_1$	A_1
$1a_1^2 2a_1^1 1b_2^2 1b_1^1$	$^3B_1$	A_2,B_2,A_1
	$^1B_1$	B_1
$1a_1^2 2a_1^2 3a_1^1 1b_2$	$^3B_2$	A_1,B_1,A_2
	$^1B_2$	B_2
$1a_1^2 2a_1 3a_1 1b_2^2$	$^3A_1$	B_1,B_2,A_2
	$^1A_1$	A_1
$1a_1^2 2a_1^2 1b_2^1 1b_1^1$	$^3A_2$	A_1,B_1,B_2
	$^1A_2$	A_2
$1a_1^2 2a_1 1b_2^2 1a_2$	$^3A_2$	A_1,B_1,B_2
	$^1A_2$	A_2
$1a_1^2 2a_1^2 3a_1 1b_2$	$^3B_2$	A_1,B_1,A_2
	$^1B_2$	B_2

be described by the leading $1a_1^2 2a_1\alpha 1b_2^2 1b_1\beta$ and $1a_1^2 2a_1\beta 1b_2^2 1b_1\alpha$ configurations. These two configurations also describe the $^1B_1(B_1)$ state with opposite sign. Thus our RCI calculations included all the reference configurations listed in Table V with appropriate spins for the open shells which describe the electronic state we seek.

The CASSCF/SOCI calculations were carried out using a version of ALCHEMY II codes,[29] modified to include the relativistic effective potentials as described in Ref. 8. The spin–orbit integrals in Gaussian basis sets were obtained using Pitzer's modified version of ARGOS.[23] The RCI calculations were carried out using the a modified and enhanced version of a code for diatomics based on the method in Ref. 14.

III. RESULTS AND DISCUSSION

We first discuss the properties of the electronic states of GeH_2, SnH_2, and PbH_2 separately and then compare them.

TABLE V. List of reference configuration included in the RCI calculations.

State	Reference configurations[a]
$^1A_1(A_1)$	$1a_1^2 2a_1^2 1b_2^2(1), 1a_1^2 2a_1 3a_1 1b_2 2b_2(6),$ $1a_1^2 2a_1^2 2b_2^2(1), 1a_1^2 2a_1 1b_2^2 1b_1(2),$ $1a_1^2 2a_1^2 3a_1 1b_1(2), 1a_1^2 2a_1 1b_2^2 1a_2(2)$ $1a_1^2 2a_1^2 1b_2 1b_1(2), 1a_1^2 2a_1^2 3a_1 1b_2(2)$
$^3B_1(A_2)$	$1a_1^2 2a_1 1b_2^2 1b_1(2), 1a_1^2 2a_1^2 3a_1 1b_1(2), 1a_1^2 2a_1^2 3a_1 1b_2(2),$ $1a_1^2 2a_1 1b_2^2 2b_2(2), 1a_1^2 2a_1^2 1b_2 1b_1(2),$ $1a_1^2 2a_1 1b_2^2 1a_2(2), 1a_1^2 2a_1 3a_1 1b_2^2(2)$
$^3B_1(B_2)$	$1a_1^2 2a_1 1b_2^2 1b_1(2), 1a_1^2 2a_1^2 3a_1 1b_1(2),$ $1a_1^2 2a_1^2 3a_1 1b_2(2), 1a_1^2 2a_1 1b_2^2 2b_2(2),$ $1a_1^2 2a_1^2 1b_2 1b_1(2), 1a_1^2 2a_1 1b_2^2 1a_2(2),$ $1a_1^2 2a_1 3a_1 1b_2^2(2)$
$^3B_1(A_1)$	$1a_1^2 2a_1 1b_2^2 1b_1(2), 1a_1^2 2a_1^2 1b_2^2(1), 1a_1^2 2a_1 3a_1 1b_2 2b_2(6),$ $1a_1^2 2a_1^2 2b_2^2(1), 1a_1^2 2a_1^2 3a_1 1b_1(2),$ $1a_1^2 2a_1 1b_2^2 1a_2(2), 1a_1^2 2a_1^2 1b_2 1b_1(2), 1a_1^2 2a_1^2 3a_1 1b_2(2),$
$^1B_1(B_1)$	$1a_1^2 2a_1 1b_2^2 1b_1(2), 1a_1^2 2a_1^2 3a_1 1b_1(2), 1a_1^2 2a_1 1b_2 2b_2 1b_1(6),$ $1a_1^2 2a_1^2 1b_2 1b_1(2), 1a_1^2 2a_1 1b_2^2 1a_2(2), 1a_1^2 2a_1 3a_1 1b_2^2(2),$ $1a_1^2 2a_1^2 3a_1^2 1b_2(2), 1a_1^2 2a_1 1b_2^2 2b_2(2)$

[a] Numbers in parentheses indicate the different spin configurations included in the RCI for the listed spatial configuration.

In the section on comparison we also discuss the nature of CI wave functions, spin–orbit contaminations, and the Mulliken population analyses of all three species considered in this investigation. The geometries of the various electronic states of PbH_2 are shown in Fig. 1 since the spin–orbit effects influence the geometries of the various electronic states of PbH_2 to a considerable extent.

A. GeH_2

The calculated properties of GeH_2 with the MCSCF/SOCI/RCI schemes are shown in Table VI. The electronic states are designated in both C_{2v} and C_{2v}^2 groups. The state in parentheses is the appropriate state including the spin–orbit term (the symmetry in the double group). As one can see from Table VI, the ground state of GeH_2 is of $^1A_1$ symmetry as expected. The spin–orbit correction for the ground state is negligible. The geometry changes due to the spin–orbit operator are also negligible for GeH_2. The largest splitting due to the spin–orbit operator is for the $^3B_1$ state and is about 0.12 kcal/mol, with the A_1 component of $^3B_1$ being the lowest. The spin–orbit contamination of the A_1 components of $^1A_1$ and $^3B_1$ is not significant for GeH_2.

The bond lengths and the bond angles of the electronic states of GeH_2 exhibit remarkable resemblance to the corresponding states of SiH_2. For example, all electron CASSCF/SOCI calculations which included f functions in the basis set yielded $r_e = 1.520$, $\theta_e = 92.7°$ for the $X\ ^1A_1$ state of SiH_2.[5] The Ge–H bond length of 1.587 Å and $\theta_e = 91.5°$ for the $X\ ^1A_1$ state of GeH_2 is only a bit different from SiH_2 if one adjusts the SiH bond length for GeH.

The dipole moment of the $X\ ^1A_1$ ground state was calculated from the SOCI natural orbitals. Thus we believe that this value is quite reliable. Moreover, similar calculations on the diatomic GeH with the same relativistic effective potentials yielded a dipole moment of 0.0976 D[13] in comparison to

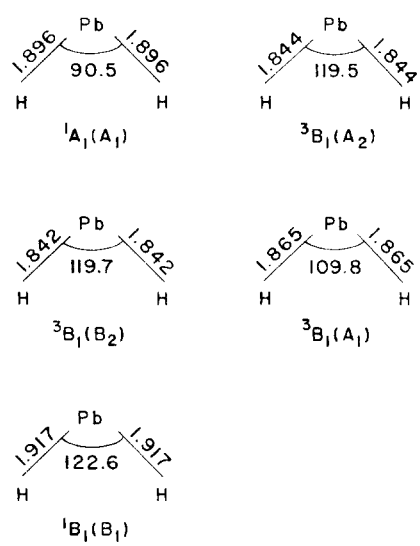

FIG. 1 The predicted geometries including the spin–orbit coupling effects of PbH_2.

TABLE VI. Structures and properties of GeH_2.

State	R_e (Å)	θ_e (deg)	T_e[a] (kcal/mol)	μ_e (D)
$^1A_1(A_1)$	1.587	91.5	0	...
$^1A_1$	1.587	91.5	0.05	0.1586
$^3B_1(A_1)$	1.534	119.8	23.05(22.95)	
$^3B_1(A_2)$	1.534	119.8	23.17(23.07)	
$^3B_1(B_2)$	1.534	119.8	23.17(23.07)	
$^3B_1$	1.534	119.8	23.2 (23.1)	0.004
$^1B_1(B_1)$	1.553	122.1	47.56(47.26)	
$^1B_1$	1.553	122.1	47.6(47.3)	0.016

[a] Energy separations in parentheses include Davidson's correction for higher-order unlinked cluster configurations. The states with labels in parentheses are spin–orbit states while the states without those labels are obtained without the spin–orbit term.

all-electron CEPA dipole moment of 0.093 D.[11] In this investigation we have not studied the effect of spin–orbit interaction on the dipole moments since our codes have not yet been modified to do that. However, earlier calculations on GeH[13] revealed that the effect of spin–orbit coupling on the dipole moment is only 0.5%. The spin–orbit coupling tends to decrease the μ_e value of GeH by this amount. Based on this finding, we believe the dipole moments reported in Table VI would be changed at most by 1% by the spin–orbit coupling term.

The singlet–triplet energy separation of GeH_2 (23 kcal/mol) is not far from the corresponding splitting for SiH_2[5] (19.6 kcal/mol). The slightly larger value is consistent with the outer s^2p^2–sp^3 splittings of the Si(48 500 cm^{-1}) and Ge ($>56\,000$ cm^{-1}) atoms.[30] Since the formation of $^3B_1$ from $^1A_1$ involves excitation from the outer s orbital into the p orbital, the $^1A_1$–$^3B_1$ splitting is a bit larger for GeH_2.

The nature of the electronic states, Mulliken population analysis, and related details will be discussed in Sec. III D.

B. SnH_2

The calculated structures and electronic properties of SnH_2 are shown in Table VII. As can be seen from Table VII, the ordering of the electronic states of SnH_2 is consistent with the corresponding ordering for GeH_2.

The singlet–triplet energy separation of SnH_2 is about 25 kcal/mol. This value is only 2.5 kcal/mol higher than our previous CASSCF/SOCI calculations[17] which employed a somewhat smaller ($3s3p2d$) basis set. Thus it is gratifying to note that the addition of s-, p-, and two d-type diffuse functions, do not change this splitting by more than 2.5 kcal/mol. The present $^1A_1$–$^1B_1$ splitting of 46 kcal/mol also differs by about the same factor (2.5 kcal) but in the opposite direction. This is consistent with the calculations on SiH_2[5] which revealed that higher order correlation effects and extension of basis sets increased the $^1A_1$–$^3B_1$ splitting but decreased the $^1A_1$–$^1B_1$ splitting.

The effect of spin–orbit coupling on energies is larger for SnH_2. Specifically, the ground state is lowered by 0.4 kcal/mol primarily due to the stabilization induced by contamination with other electronic states which ordinarily do not mix in the absence of the spin–orbit term. The splitting of the excited $^3B_1$ state into A_1, A_2, and B_2 components is 0.9 kcal/mol. Note that the A_1 component is lowered more in comparison to the B_1 and B_2 components. This is anticipated if the contamination with other electronic states is not very large. This is also consistent with our earlier prediction[8] that the A_1 state would be lower for SnH_2. Thus in the absence of the spin–orbit contaminations A_1 would be lower and the splitting between A_2 and B_2 should be smaller if the bond angle is obtuse. The actual spin–orbit splitting is consistent with this qualitative prediction.

The striking effect of the spin–orbit term is on the geometry of the A_1 component of the $^3B_1$ state. This is even larger for PbH_2. The A_1 component of $^3B_1$ mixes with the A_1 component of the X $^1A_1$ ground state to a considerable extent for PbH_2 and SnH_2. This mixing is negligible for GeH_2. Thus no geometry change is brought about for GeH_2. For SnH_2 however, the bond angle is reduced by almost 3.5°. The actual magnitude of this contamination will be discussed later.

The calculated dipole moments of all the three states of SnH_2 indicate that the metal atom carries the positive charge in these electronic states. The ground state has a larger dipole moment in comparison to the excited states. The earlier investigation on the dipole moment of SnH by Chapman *et al.*[13] reveals that the μ_e value is lowered by about 1.5% due to the spin–orbit term. Thus, we believe, the reported dipole moments in Table VII without the spin–orbit term should be accurate to this degree.

TABLE VII. Structures and properties of electronic states of SnH_2.[a]

State	R_e (Å)	θ_e (deg)	T_e (kcal/mol)	μ_e (D)
$^1A_1(A_1)$	1.785	91.1	0	
$^1A_1$	1.785	91.1	0.36	0.554
$^3B_1(A_1)$	1.730	114.9	23.8(23.7)	
$^3B_1(A_2)$	1.728	118.4	24.69(24.65)	
$^3B_1(B_2)$	1.728	118.4	24.68(24.66)	
$^3B_1$	1.728	118.4	24.90(24.86)	0.271
$^1B_1(B_1)$	1.754	121.4	45.8(45.0)	
$^1B_1$	1.754	121.4	46.1(45.3)	0.186

[a] Numbers in parentheses are energy separations which included the Davidson correction for uncoupled clusters. The states with labels in parentheses are spin–orbit states while the states without these labels were obtained without the spin–orbit term.

C. PbH_2

The calculated geometries, energy separations, and dipole moments of the various electronic states of PbH_2 are shown in Table VIII.

As one can see from Table VIII, the X $^1A_1$–$^3B_1$ splitting in the absence of the spin–orbit term is considerably larger (37 kcal/mol) for PbH_2 in comparison to the lighter analogs. This is primarily a consequence of the fact that the relativistic mass–velocity contraction stabilizes the outer $6s$ orbital of the atoms in that row. Consequently, the $6s^2$ shell is relatively inert, a phenomenon referred to as the "inert pair" effect which is actually a relativistic effect. Since the X $^1A_1$–$^3B_1$ splitting depends on a partial excitation of the $6s$ electron

TABLE VIII. Structure and properties of electronic states of PbH_2.

State	R_e (Å)	θ_e (deg)	T_e[a] (kcal/mol)	μ_e (D)
$^1A_1(A_1)$	1.896	90.5	0	...
$^1A_1$	1.896	90.5	3.74	1.368
$^3B_1(A_2)$	1.844	119.5	34.4(34.1)	...
$^3B_1(B_2)$	1.842	119.7	34.6(34.3)	...
$^3B_1(A_1)$	1.865	109.8	40.8(40.6)	...
$^3B_1$	1.838	119.5	36.9(36.6)	0.385
$^1B_1(B_1)$	1.917	122.6	49.5(49.1)	...
$^1B_1$	1.903	122	52.4(52.0)	0.53

[a] Numbers in parentheses include Davidson's correction. The states with labels in parentheses are spin–orbit states while the states without labels in parentheses were obtained without the spin–orbit term.

into the $6p$ orbital, the $^3B_1$ state of PbH_2 is considerably higher in energy.

The effect of spin–orbit coupling on PbH_2 is very significant as one can see from Table VIII and Fig. 1. Even the closed shell $^1A_1$ ground state is lowered by 4 kcal/mol due to the spin–orbit coupling. This lowering is primarily due to contamination with other electronic states which do not mix in the absence of the spin–orbit term (spin–orbit contamination). The excited $^3B_1$ state is split apart into the A_2, B_2, and A_1 components. This splitting is 6.4 kcal/mol, which is about 16% of the singlet–triplet energy separation in the absence of the spin–orbit term. The $^1B_1$ state is lowered by 3 kcal/mol due to the spin–orbit term.

The geometry of the A_1 component of $^3B_1$ changes dramatically (see Fig. 1) due to contamination with the $\mathbf{X}\ ^1A_1$ ground state induced by the spin–orbit coupling. The bond angle of this state decreases by almost 10° (8.4%). The bond length increases ($\Delta r_e = 0.027$ Å) in comparison to the $^3B_1$ state in the absence of the spin–orbit term. The increase in the bond length and the decrease in the bond angle is consistent with the fact that the ground state $\mathbf{X}\ ^1A_1$ has a larger bond length and smaller bond angle and that the $^3B_1$ (A_1) state is a mixture of $^3B_1$ and $^1A_1$.

The bond length of the $^1B_1$ state increases by 0.014 Å due to the spin–orbit term. The exact nature of these contaminations will be discussed in the next section.

The calculated dipole moments of the electronic states of PbH_2 are quite large. The positive charge is on the metal atom, which is consistent with the more metallic nature of the lead atom in comparison to Ge or Si. The effect of the spin–orbit term on the dipole moment has not been studied here due to technical reasons mentioned before. However, our earlier investigation on the diatomic lead hydride reveals that μ_e decreases by 4.5%. For PbH_2 the contamination between $^1A_1$ and $^3B_1$ would bring about an appreciable change in the dipole moments. Thus the dipole moments reported in Table VIII for PbH_2 should not be considered

TABLE IX. Coefficients of the leading configurations in the SOCI wave function of the electronic states of GeH_2, SnH_2, and PbH_2.

Molecule	State	Coefficient	$1a_1$	$2a_1$	$3a_1$	$1b_2$	$2b_2$	$1b_1$	$2b_1$	$\Sigma_i C_i^2$[a]
GeH_2	$^1A_1$	0.955	2	2	0	2	0	0		0.963
		−0.147	2	0	0	2	0	2		
		−0.069	2	2	0	0	2	0		
		−0.069	2	1	1	1	1	0		
SnH_2	$^1A_1$	0.955	2	2	0	2	0	0		0.966
		−0.143	2	0	0	2	0	2		
		−0.077	2	1	1	1	1	0		
		−0.073	2	2	0	0	2	0		
PbH_2	$^1A_1$	0.959	2	2	0	2	0	0		0.974
		0.107	2	1	1	1	1	0		
		0.082	2	2	0	0	2	0		
		0.073	1	1	0	2	0	2		
GeH_2	$^3B_1$	−0.967	2	1	0	2	0	1		0.962
		0.069	2	1	2	0	0	1		
SnH_2	$^3B_1$	0.965	2	1	0	2	0	1		0.965
		−0.073	2	1	2	0	0	1		
		−0.066	2	2	1	0	0	1		
PbH_2	$^3B_1$	0.961	2	1	0	2	0	1	0	0.968
		0.095	2	2	1	0	0	1	0	
		0.081	2	1	2	0	0	1	0	
GeH_2	$^1B_1$	0.958	2	1	0	2	0	1	0	0.957
		−0.097	1	1	1	2	0	1	0	
		0.063	2	1	2	0	0	1	0	
SnH_2	$^1B_1$	0.941	2	1	0	2	0	1	0	0.943
		−0.105	1	2	0	2	0	1	0	
		−0.104	2	1	0	2	0	0	1	
		−0.094	1	1	1	2	0	1	0	
PbH_2	$^1B_1$	0.948	2	1	0	2	0	1	0	0.966
		−0.136	2	1	0	1	1	1	0	
		0.102	1	1	1	2	0	1	0	
		0.100	2	2	1	0	0	1	0	

[a] $\Sigma_i C_i^2$ is the sum of the coefficients of the CASSCF reference configurations in the SOCI calculations.

very accurate, but we believe that the largest correction would be for the $^3B_1$ (A_1) component, since the geometry of this state changes dramatically due to the spin–orbit term.

D. Comparison of the nature of the electronic states of GeH_2, SnH_2, and PbH_2

Table IX shows the coefficients of the leading configurations of the three electronic states of GeH_2, SnH_2, and PbH_2 in the absence of the spin–orbit term. The similarity between GeH_2 and SnH_2 is noticeable even in the contributions of the most important configurations. In that table we have also included the sum of the squares of the coefficients of the CASSCF reference configurations in the SOCI. This approximately measures the importance of the higher order configurations not included in the CASSCF. For a given species, the smallest sum is for the $^1B_1$ excited state and the largest sum is for the ground state. This trend is also consistent with the Davidson's correction which is largest for the excited $^1B_1$ state. This is especially so for SnH_2. In comparing different radicals for a given electronic state we find that PbH_2 has the largest $\Sigma_i C_i$.[2] The second and third important configurations are not always the same for different species.

Table X gives the gross and overlap Mulliken population analyses for the various electronic states of GeH_2, SnH_2, and PbH_2. The Mulliken population analyses were carried out without the f-type polarization functions since the ALCHEMY property integral codes do not have the capabilities to include the f functions at present. The d population in that table is corrected for the $d_{x^2+y^2+z^2}(3s)$ population. The total gross population on the metal atom provides some idea about the nature of the bond (ionic or covalent). As one can see from Table X, the gross population of the metal atom is the smallest for the tin atom and the largest for germanium. Thus, the Sn–H bond appears to be most ionic for SnH_2 in comparing the triads. However, the calculated dipole moment is largest for PbH_2 since the dipole moment depends both on the magnitude of charges and their separation. The Pb–H bond lengths are considerably larger than the Sn–H bond lengths in MH_2.

The heavy atom s, p, and d populations in the various electronic states are also of interest. In general, the $^1A_1$ state has a larger s population than the $^3B_1$ and $^1B_1$ states. This is consistent with the qualitative description that the $^1A_1$ state arises from s^2p^2 configuration while the $^3B_1$ and $^1B_1$ states arise from the sp^3 configuration of the heavy atom.

The "inert pair" effect for PbH_2 can be seen in the s population of the lead atom. The s population of PbH_2 in all electronic states is considerably larger especially for the $^3B_1$ and $^1B_1$ states. For the ground state the s population of PbH_2 is larger than GeH_2 and SnH_2, but this difference is somewhat smaller in comparison to the excited $^3B_1$ and $^1B_1$ states. As discussed earlier the larger s population for the lead atom is primarily due to the relativistic mass–velocity stabilization of the outer $6s$ orbital of the lead atom. Thus the $6s$–$6p$ promotion energy is considerably larger for Pb.

The metal–hydrogen overlap population is the largest for GeH_2 in comparing corresponding states and the smallest for PbH_2. Thus the bonding appears to be strongest in GeH_2 in comparing the triads although the overlap populations should not be used as the ultimate measures of the strength of bonding. However, it is interesting that the $^3B_1$ state of SnH_2 and GeH_2 have larger overlaps in comparison to $^1A_1$ while the order is reversed for PbH_2.

Table XI shows the analysis of the relativistic CI wave functions for the various spin–orbit states of the three species. We have grouped the corresponding states of the three species together to contrast the spin–orbit contaminations.

The ground state $^1A_1$ (A_1) is relatively pure for SnH_2 and GeH_2 while for PbH_2 contamination from the excited $^3B_1$ and $^3A_2$ is nonnegligible. Similarly, the A_2 and B_2 components of $^3B_1$ are relatively pure. The singlet–triplet mixing in the $^3B_1$ (B_2) is about 0.2% for PbH_2 while the spin–orbit contamination from $^3B_2$ (A_2) and $^3A_1$ (A_2) adds up to 0.8% for PbH_2.

The $^3B_1$ (A_1) state undergoes considerable mixing with the $^1A_1$ state for PbH_2 and SnH_2. The singlet–triplet ($^1A_1$–$^3B_1$) mixing for PbH_2 near the (r_e, θ_e) of the $^3B_1(A_1)$ state is 24% as one can see from Table XI. The corresponding percentage for SnH_2 is 6%. This contamination of the ground state by the $^3B_1$ (A_1) component is manifested in the geometries and energies of the $^3B_1$ (A_1) components of the two species as one can see from Tables VII and VIII. The geometry of the $^3B_1$ (A_1) component moves towards the ground state geometry for both PbH_2 and SnH_2. The change is larger for PbH_2 since the contamination is larger. This contamination is so large that it moves the A_1 component up relative to the $^3B_1$ state for PbH_2. The other interesting aspect of spin–orbit contamination is that for PbH_2 even at the equilibrium geometry of $^3B_1$, the $^1A_1$ state is considerably lower. Thus $^3B_1$ (A_1) is the second root of the RCI calculations of the A_1 state. For SnH_2, however, the A_1 component of $^3B_1$ comes out to be the first root primarily becaue the $^1A_1$–$^3B_1$ splitting is lower at the equilibrium geometry of $^3B_1$. Thus, $^3B_1$ (A_1) is lowered with respect to $^3B_1$ for SnH_2, but is raised with respect to $^3B_1$ for PbH_2.

TABLE X. Mulliken population analysis for the electronic states of PbH_2, SnH_2, and GeH_2.

Molecule	State	Gross M	Gross H	M(s)	M(p)	M(d)	Overlap M–H
PbH_2	$^1A_1$	13.80	2.20	1.876	1.865	10.06	1.158
PbH_2	$^3B_1$	13.978	2.022	1.649	2.276	10.05	1.084
PbH_2	$^1B_1$	13.979	2.021	1.776	2.153	10.05	0.814
SnH_2	$^1A_1$	13.744	2.256	1.848	1.882	10.01	1.214
SnH_2	$^3B_1$	13.887	2.113	1.467	2.361	10.06	1.254
SnH_2	$^1B_1$	13.939	2.061	1.646	2.288	10.05	1.045
GeH_2	$^1A_1$	13.877	2.124	1.758	2.006	10.11	1.254
GeH_2	$^3B_1$	13.997	2.003	1.486	2.454	10.08	1.314
GeH_2	$^1B_1$	14.05	1.95	1.592	2.396	10.06	1.123

IV. CONCLUSIONS

In this investigation we made calculations on the three lowest states and their spin–orbit components of GeH_2,

TABLE XI. The weights of the various electronic states in relativisitic CI of GeH_2, SnH_2, and PbH_2.

Molecule	Relativistic state	Weights in percentage
PbH_2	$^1A_1(A_1)$	$1a_1^2 2a_1^2 1b_2^2\ ^1A_1(91), 1a_1^2 2a_1^1 1b_2^2 1b_1^1\ ^3B_1(A_1)(1.2)$, $1a_1^2 2a_1^2 1b_2^1 1b_1^1\ ^3A_2(A_1)(0.73)$
SnH_2	$^1A_1(A_1)$	$1a_1^2 2a_1^2 1b_2^2\ ^1A_1(93)$, $1a_1^2 2a_1^2 1b_2^1 1b_1\ ^3A_2(A_1)(0.05)$
GeH_2	$^1A_1(A_1)$	$1a_1^2 2a_1^2 1b_2^2\ ^1A_1(93)$
PbH_2	$^3B_1(A_2)$	$1a_1^2 2a_1^1 1b_2^2 1b_1^1\ ^3B_1(A_2)(92), 1a_1^2 2a_1 1b_2^2 2b_2\ ^3B_2(A_2)(0.4)$, $1a_1^2 2a_1^2 3a_1^1 1b_1^1\ ^3B_1(A_2)(0.8), 1a_1^2 2a_1 3a_1 1b_2^2\ ^3A_1(A_2)(0.4)$
SnH_2	$^3B_1(A_2)$	$1a_1^2 2a_1 1b_2^2 1b_1\ ^3B_1(A_2)(95)$
GeH_2	$^3B_1(A_2)$	$1a_1^2 2a_1 1b_2^2 1b_1\ ^3B_1(A_2)(95)$
PbH_2	$^3B_1(A_1)$	$1a_1^2 2a_1 1b_2^2 1b_1^1\ ^3B_1(A_1)(67), 1a_1^2 2a_1^2 1b_2^2\ ^1A_1(A_1)(24)$, $1a_1^2 1b_2^2 1b_1^2\ ^1A_1(A_1)(1.3), 1a_1^2 2a_1^2 3a_1 1b_2\ ^3B_2(A_1)(0.1)$, $1a_1^2 2a_1^2 3a_1 1b_1\ ^3B_1(A_1)(0.7)$
SnH_2	$^3B_1(A_1)$	$1a_1^2 2a_1 1b_2^2 1b_1^1\ ^3B_1(A_1)(89), 1a_1^2 2a_1^2 1b_2^2\ ^1A_1(A_1)(5.7)$
GeH_2	$^3B_1(A_1)$	$1a_1^2 2a_1 1b_2^2 1b_1\ ^3B_1(A_1)(94), 1a_1^2 2a_1^2 1b_2^2\ ^1A_1(A_1)(0.8)$
PbH_2	$^3B_1(B_2)$	$1a_1^2 2a_1 1b_2^2 1b_1\ ^3B_1(93), 1a_1^2 2a_1 1b_2^2 2b_2\ ^1B_2(0.2)$
SnH_2	$^3B_1(B_2)$	$1a_1^2 2a_1 1b_2^2 1b_1\ ^3B_1(94)$
GeH_2	$^3B_1(B_2)$	$1a_1^2 2a_1 1b_2^2 1b_1\ ^3B_1(95)$
PbH_2	$^1B_1(B_1)$	$1a_1^2 2a_1 1b_2^2 1b_1\ ^1B_1(90), 1a_1^2 2a_1 1b_2 2b_1 1b_1\ ^1B_1(1.2)$, $1a_1^2 2a_1 3a_1 1b_2^2\ ^3A_1(B_1)(0.85), 1a_1^2 2a_1 1b_2^2 2b_2\ ^3B_2(B_1)(0.85)$
SnH_2	$^1B_1(B_1)$	$1a_1^2 2a_1 1b_2^2 1b_1\ ^1B_1(93)$
GeH_2	$^1B_1(B_1)$	$1a_1^2 2a_1 1b_2^2 1b_1\ ^1B_1(94)$

SnH_2, and PbH_2. A scheme to include both correlation and spin–orbit corrections was developed for polyatomics based on CASSCF/CI/RCI methodology. The spin–orbit effects were found to be important for PbH_2 and SnH_2 and small for GeH_2. The most important impact of the spin–orbit term was found to be on the geometry and energy of the A_1 component of the $^3B_1$ state. The $^1A_1$–$^3B_1$ mixing was found to be significant for PbH_2 (24%) and SnH_2 (6%). The geometries, energy separations and dipole moments of the low-lying electronic states of GeH_2, SnH_2, and PbH_2 are predicted.

ACKNOWLEDGMENTS

This research was supported in part by the National Science Foundation Grant No. CHE8520556. The author would like to thank Professor Russel Pitzer for many illuminating discussions during this investigation and a referee for many useful comments on this manuscript.

[1]A. R. W. Mckellar, P. R. Bunker, T. J. Sears, K. M. Evenson, R. S. Saykally, and S. R. Langhoff, J. Chem. Phys. **79**, 5251 (1983) (complete set of references before 1983 on CH_2 is in this reference).
[2]D. G. Leopold, K. Murray, A. E. S. Miller, and W. C. Lineberger, J. Chem. Phys. **83**, 4849 (1985).
[3]M. Colvin, R. S. Grev, H. F. Schaefer III, and J. Bicerano, Chem. Phys. Lett. **99**, 399 (1983).
[4]J. Rice and N. C. Handy, Chem. Phys. Lett. **107**, 365 (1984).
[5]K. Balasubramanian and A. D. McLean, J. Chem. Phys. **85**, 5117 (1986).
[6]R. A. Phillips, R. J. Buenker, R. Beardsworth, P. R. Bunker, P. Jensen, and W. P. Kraemer, Chem. Phys. Lett. **118**, 60 (1985).
[7]L. G. M. Pettersson and P. E. M. Siegbahn, Chem. Phys. **105**, 355 (1986).
[8]K. Balasubramanian, Chem. Phys. Lett. **127**, 585 (1986).
[9]J. F. Harrison, J. Am. Chem. Soc. **103**, 7406 (1981).
[10]J. M. Brown, K. M. Evenson, and T. J. Sears, J. Chem. Phys. **83**, 3275 (1985).
[11]H. J. Werner and A. D. Buckingham, Chem. Phys. Lett. **125**, 433 (1986).
[12]L. G. M. Pettersson and S. R. Langhoff, Chem. Phys. Lett. **125**, 429 (1986).
[13]D. A. Chapman, K. Balasubramanian, J. Q. Li, and S. H. Lin, J. Chem. Phys. **88**, 3826 (1988).
[14]P. A. Christiansen, K. Balasubramanian,and K. S. Pitzer, J. Chem. Phys. **76**, 5087 (1982).
[15]K. Balasubramanian and K. S. Pitzer, Adv. Chem. Phys. **67**, 287 (1987); P. A. Christiansen, W. C. Ermler, and K. S. Pitzer, Annu. Rev. Phys. Chem. **36**, 407 (1985).
[16]Y. S. Lee, W. C. Ermler, and K. S. Pitzer, J. Chem. Phys. **67**, 5861 (1977).
[17]P. A. Christiansen, Y. S. Lee, and K. S. Pitzer, J. Chem. Phys. **71**, 445 (1979).
[18]W. C. Ermler, Y. S. Lee, P. A. Christiansen, and K. S. Pitzer, Chem. Phys. Lett. **81**, 70 (1981).
[19]P. Hafner and W. H. E. Schwarz, Chem. Phys. Lett. **65**, 537 (1979).
[20]M. M. Hurley, L. F. Pacios, P. A. Christiansen, R. B. Ross, and W. C. Ermler, J. Chem. Phys. **87**, 2812 (1987).
[21]L. A. LaJohn, P. A. Christiansen, R. B. Ross, T. Atashroo, and W. C. Ermler, J. Chem. Phys. **87**, 2812 (1987).
[22]W. C. Ermler and P. A. Christiansen (private communication).
[23]R. M. Pitzer and N. W. Winter, J. Phys. Chem. **92**, 3061 (1988).
[24]J. Paldus, in *Theoretical Chemistry: Advances and Perspectives*, edited by H. Eyring and D. J. Henderson (Academic, New York, 1976).
[25]I. Shavitt, Int. J. Quantum Chem. Symp. **12**, 5 (1978).
[26]B. R. Brooks and H. F. Schaefer III, J. Chem. Phys. **70**, 5092 (1979).
[27]M. Yoshimine and B. Liu, J. Chem. Phys. **74**, 612 (1981).
[28]S. R. Langhoff and E. R. Davidson, Int. J. Quantum Chem. **8**, 61 (1974).
[29]The major authors of ALCHEMY II codes are B. Lengsfield, B. Liu, and M. Yoshimine.
[30]C. E. Moore, *Tables of Atomic Energy Levels*, Natl. Bur. Stand. Circ. 467 (U.S. GPO, Washington, DC, 1971), Vols. I–III.